Physicochemical and rheo-mechanical properties of titanium dioxide reinforced sage seed gum nanohybrid hydrogel

Seyed Amir Oleyaei[a], Seyed Mohammad Ali Razavi[a,*], Kirsi S. Mikkonen[b]

[a]*Food Hydrocolloids Research Centre, Department of Food Science and Technology, Ferdowsi University of Mashhad (FUM), P.O. Box 91775-1163, Mashhad, Iran*

[b]*Department of Food and Nutrition, P.O. Box 66 (Agnes Sjöberginkatu 2), FI-00014, University of Helsinki, Finland*

Abstract

Sage seed gum (SSG) is a promising biopolymer candidate for utilization and substitution prevalent galactomannan gels of interest in soft biomaterial applications. Herein, physicochemical and rheo-mechanical properties of SSG matrix reinforced by various titanium dioxide (TiO_2) nanoparticles loading (0-25 wt%) were monitored. Particle size and density of the nanocomposite increased with raising TiO_2 content, due to the creation of more compact agglomerated and aggregated microstructure. Increasing the particle size resulted in lower electrophoretic mobility of SSG-TiO_2 systems upon nanoparticles addition, confirmed the adsorption of TiO_2 on the SSG macromolecule. Mechanical spectra of the SSG-based nanocomposites demonstrated a more solid-like behavior by lower frequency-dependent viscoelastic moduli, suggested a structural decoration of the nanohybrid gels discussed in terms of polymer bridging effect and formation of percolated matrix-particle superstructure. Crucial textural parameters improved with increasing TiO_2 until a

*Corresponding author: Tel: +98-51-38805763, Fax: +98-51-38787430, Email: s.razavi@um.ac.ir

critical level (15 wt%), after which further increments in filler resulted in a reduction of hardness, adhesiveness and apparent modulus of elasticity. Deformation of rod-like junction zones acting as physical crosslinks in the system and fracture theory were used to explain the strain-stiffening and adhesive behavior of SSG-based gels, respectively. The nanocomposite gels with tunable functional properties might be ideal candidates for biomaterial industry.

Keywords: Biomaterial; Hydrogel; Galactomannan; Nanocomposite; Rheology; Titanium dioxide.

1. Introduction

Hydrogels are three-dimensional (3D) polymer networks containing large quantities of water or biological fluids, which have attracted much attention as functional soft materials. They are used for several applications ranging from biomedical to agricultural and food industries [1]. Hydrogels can also proffer novel opportunities for the design of more efficient polymer-based substances with applicable characteristics, by converting into the highly porous engineered scaffold, aerogel and thin film constructs [2–4]. Nowadays, there is a great consideration in developing special hydrogels from non-toxic natural hydrophilic polymers (hydrocolloids) with low cost and appropriate functionality. Galactomannan polysaccharides such as sage seed gum (SSG) are the ones which could meet these appeals. SSG with a 1.78-1.93:1 mannose/galactose ratio, 28-32% uronic acids (as galacturonic acid equivalent) and the weight average molecular weight of 1.5×10^6 Da is similar to guar gum and shows a polyelectrolyte behavior [5]. Sage seed gum adopts a self-structured rigid rod conformation in aqueous solution with more chain stiffness in comparison to xanthan gum. SSG dispersion demonstrates higher yield stress, pseudoplasticity, zero-shear

2

viscosity and thermal stability compared with guar and xanthan gums [6]. According to described properties, SSG is an engrossing option to substitute commercial hydrocolloids in food, cosmetics, and pharmaceutical systems. However, most natural hydrocolloids present a weak network structure, so the preparation of high-strength SSG-based hydrogel for practical applications is challenging. Nanocomposite gel fabrication, using organic/inorganic nanoparticles (NPs) as reinforcing filler or cross-linker agent in a polymer matrix, is a new interesting strategy to overcome the shortcoming and developing novel hydrogels with tailorable and modified properties. Compared with the other attempts such as topological and double network gel production, which recently were made to design hydrogels with improved mechanical properties, the nanocomposite gel had the advantages of economy, stability, and simplicity of synthesis [7]. A key attribute of many bio-based nanohybrid hydrogels is their mechanical viscoelastic nature, which mimics hydrogel behavior as an intermediary commodity or final product. Besides, the formulation, ultimate characteristics, economic features of the process and shelf life of finished products are rheo-mechanical dependent factors [8]. Therefore tuning and characterizing hydrogel rheo-textural properties as a practical approach which supplies some useful evidence about nanoparticle dispersion pattern and matrix-particle interactions, are important when creating and maintaining engineered biomaterials. A number of studies on the linear and nonlinear viscoelastic (n-LVE) properties of renewable biopolymer-based (alginate, xanthan, locust bean gum, gelatin, scleroglucan and carboxymethyl cellulose) hydrogels, mainly for reinforced with NPs (silica montmorillonite, Laponite and zinc oxide), have been indicated that strong enhancements in the elasticity and stiffness of these systems occur with rising nanofiller contents. These changes often demonstrated by transitions from liquid-like to solid-like rheological behavior at relatively low NPs loadings with a high complex viscosity (η^*) and complex modulus (G^*) [9–15]. Titanium

3

dioxide (TiO_2) is one of the best biocompatible and hydrophilic inorganic NPs, which is believed to be non-toxic, eco-friend and biosafe according to the Food and Drug Administration (FDA). Moreover, inexpensive nano-TiO_2 possess antibacterial, odor inhibition and self-cleaning activity due to its photocatalytic mechanism [16]. The functional characteristics of nanocomposites were diverse and strongly governed by biopolymer and NPs nature, as well as their molecular size, shape, surface charge density, polymer-particle affinity, interactions, and ratio. The possibility of natural biopolymer-TiO_2 interactions was approved by Fourier transform infrared (FT-IR) as mentioned in our previous works [17,18]. Large quantities of hydroxyl (-OH) groups on nano-TiO_2 surface enable it to be functionalized/grafted with organic material and biopolymer chains. In addition, TiO_2 has a strong affinity for carboxyl (-COOH) groups, and SSG chains have numerous carboxyl and hydroxyl agents, *i.e.*, a lot of potential binding sites for TiO_2-NPs surface. Furthermore, carboxylate groups on the repeating units of SSG chains can coordinate the Ti atoms on the nano-TiO_2 in three different unidentate, chelating and bridge bidentate modes [19]. The presence of hydrogen bonding (H-bonding) as an important interaction in the SSG-TiO_2 hybrid composite is expectable, which contributes to the improvement of mechanical properties. Such advantages make TiO_2-NPs an ideal inorganic reinforcing component in manufacturing SSG-based nanohybrid hydrogel with novel promising functional properties and applications. In particular, TiO_2-NPs were embedded into various forms of biopolymer matrix such as film, fluid and double-network gel [17–22]. However, most of these studies were related to the peruse of the antimicrobial activity, drug delivery, water vapor- and UV-shielding of nanocomposites and the investigations that examine the effect of nano-TiO_2 on the physicochemical and viscoelastic properties of nanocomposite forming solution (NFS) and hydrogels have been very scarce.

Nanocomposite (aerogel, tissue scaffold, and film) production using the casting/spreading technique consists of preparing the NFS followed by its molding and application onto a support, simply by pouring the NFS. Hence, it is seriously important to use an NFS with appropriate rheo-mechanical characteristics, which is obtained through an optimized matrix-filler ratio. In addition, the shelf-stability and functional features (adhesiveness and spreadability) of nanohybrid skin care creams and coating are textural-dependent properties. Thus, interested in developing SSG-TiO$_2$ nanohybrid hydrogel, this work aimed to study the effect of nanoparticle concentrations (C_{NPs}) on the rheo-mechanical and physicochemical attributes as well as understanding the microstructure-property relations in SSG-TiO$_2$ NFS by means of small and large deformation tests, along physicochemical characterization.

2. Materials and methods

2.1. Materials

The extraction of SSG was accomplished using Bostan et al. [23] procedure. P25 titanium dioxide nanoparticles (80% Anatase and 20% Rutile) was supplied by Evonik Degussa GmbH (Germany). The average diameter, particle density and surface area of TiO$_2$-NPs (as recorded by the company) were about 21 nm, 3.8 g/cm^3, and 50 ± 15 m^2.g^{-1}, respectively.

2.2. Hydrogel preparation

A series of nanocomposite hydrogels were produced by blending the TiO$_2$-NPs with the SSG matrix as follows. A stock solution of nano-TiO$_2$ (0.01 g/ml) was prepared by stirring overnight and sonication with 24 kHz Hielscher UP200H ultrasound (Hielscher Ultrasonics, Germany) for

two min at ambient temperature. 0, 5, 10, 15, 20 and 25 ml were taken from TiO_2-NPs stock solution and added to the appropriate amount of de-ionized water until 99 ml obtained with sodium azide (0.02%) as an antimicrobial preservative. SSG (1 gr) was added very slowly to NPs dispersion under intense magnetic stirring (5 min, 700 rpm), at 25 °C. Instances were kept on rotating roller mixer (Haematology Cell Mixer, Iran) for further 24 hours at ambient temperature to complete hydration and also providing enough time to react with nanoparticles for any possible configurationally changes before the experiment.

2.3. Particle size and Zeta (ζ)-potential

To determine the particle size and zeta (ζ)-potential, the SSG-based hydrogels were diluted 40 fold in de-ionized water and characterized in triplicate with a laser diffraction particle sizer (Cordouan, Vasco 3, and France) and dynamic light scattering (DLS) technique (ZetaCompact, CAD, and France), respectively at 25 °C.

2.4. Density and Surface tension

Density and surface tension of the nanocomposite samples were determined using Wilhelmy plate technique (K100, KRUSS, Germany) with a platinum-iridium plate (thickness: 0.2, width: 10 and length: 19.9 mm) at 25 °C. All SSG-TiO_2 hydrogels were kept steady for 1 h to reach equilibrium before the measurements. De-ionized water was used for calibration of the instrument before to the analysis. Surface tension and density assessments were conducted, at least, in triplicate.

2.5. Small amplitude oscillatory shear (SAOS) measurements

Small deformation oscillatory measurements were performed using Physica MCR 301 controlled strain/stress rheometer (Anton Paar, GmbH, Germany) equipped with the cone-plate geometry (4° angle, 0.206 mm gap and 50 mm diameter). The temperature was fixed at 20 ℃ using a Peltier system. Each sample was equilibrated, at least for two minutes before the rheological test and was coated around their periphery with light silicone oil to prevent water evaporation. The results of rheological measurements analyzed by Rheoplus software (Anton-Paar, version 3.21).

2.5.1. Stress sweep test

Stress sweep measurements in oscillatory shear were made over a stress range of 0.01−100 Pa in

the controlled rate mode, at a constant temperature and frequency of 20℃ and 1 Hz, respectively, to determine the linear viscoelastic (LVE) region. In addition to detailed study on dynamic rheological characteristics of SSG and SSG-TiO$_2$ hydrogels, the elastic modulus (G'$_{LVE}$), viscous modulus (G"$_{LVE}$), complex modulus (G$^*_{LVE}$), loss tangent (tan(δ)$_{LVE}$), the limiting value of stress (τ$_d$ or dynamic yield stress) at the LVE range, static yield stress (τ$_s$), flow-point stress (τ$_f$) with corresponding modulus (G$_f$: G'=G"), and the slope of the loss tangent at n-LVE range ofter flow-point (tan(δ)$_{s(n-LVE)}$) were calculated by the amplitude stress sweep test. Moreover, failure (fracture) stress (τ$_{Fr}$) and failure strain (γ$_{Fr}$) were determined by plotting elastic stress, the product of the elastic modulus and strain amplitude (G'.γ), as a function of rising stress and strain, respectively [5].

2.5.2. Frequency sweep test

The frequency sweep experiments were carried out within the LVE region (0.1 Pa), over a frequency range of 0.01-10 Hz. The mechanical spectra were characterized by the elastic modulus

(G'), viscous modulus (G"), loss tangent (tan δ), complex modulus (G^*) and complex viscosity (η^*), as a function of frequency. The frequency dependencies of G' and G" for SSG-based hydrogels were described by a power law model using Eq. (1) and Eq. (2), respectively as follows:

$$G' = K' \times (\omega)^{n'} \tag{1}$$

$$G'' = K'' \times (\omega)^{n''} \tag{2}$$

Where K' ($Pa.rad^{-n'}.s^{n'}$) and K'' ($Pa.rad^{-n''}.s^{n''}$) are intercepts, n' and n'' are frequency exponents, and ω is the angular velocity ($rad.s^{-1}$). Besides, the material stiffness parameter (A_α ($Pa.rad^{-\alpha}.s^{a}$)) and the order of relaxation function (α (dimensionless)) were determined by applying the Friedrich and Heymann [24] model (Eq. 3) on the complex modulus (G^*) data:

$$G^* = A_\alpha \times (\omega)^{\alpha} \tag{3}$$

2.6. Large deformation mechanical test

Large deformation behavior of SSG-TiO_2 hydrogels was investigated by the texture profile analysis (TPA) test, using a Brookfield Texture Analyzer (CT3, USA) according to a previously published method [25]. Experiments were carried out triplicate in a standard size back extrusion container disk (30 mm diameter; 45 mm length). The disk was proceeded at a rate of 1 mm/s to penetrate twice into the gel to 40% degree of compression for the pre- and post-test (recovery time was zero) at ambient temperature. The slope of the linear region of the stress-strain curve was considered as the initial tangent modulus or apparent modulus of elasticity (E_a (g/s)). Other crucial parameters such as hardness (peak force during the initial compression cycle (g)), adhesiveness (negative force area of the initial cycle (mJ)), cohesiveness (ratio of the area under the second and first compression (dimensionless)), springiness (distance from the target deformation of primary

cycle to the trigger point of second cycle (cm)), and gumminess (hardness $\times$ cohesiveness (g)) of hydrogels were obtained.

2.7. Statistical analysis

All data were analyzed statistically based on a completely randomized factorial design using analysis of variance (ANOVA) procedure in SPSS software (Version19, Chicago, IL). The Duncan Duncan's Multiple-Region test was performed to determine the differences between mean values in case of significance ($P < 0.05$).

3. Results and discussion

3.1. Particle size

Particle size measurement is a vital item in forecasting the rheological and electrophoretic behavior (ζ-potential) besides surface activity of the material. The average particle size of pure TiO_2 and SSG were 21 and 277 nm, respectively. As C_{NPs} increased to 5 and 10 wt%, the particle size increased abruptly to 499 and 764 nm, respectively (Table 1). The order of increasing particle size did not follow the order of NPs addition i.e., slowed down for high nano-TiO_2 content. From zero to 25 wt% nano-TiO_2, the composite size increased by about 264%. At $C_{NPs} = 5$ wt%, the particle size of SSG-5TiO_2 was 1.8-fold higher than that of plain SSG, but of the same order as the addition of 5 wt% TiO_2; at SSG-10TiO_2 nanocomposite, the composite size was 1.5-fold higher than SSG-5TiO_2. Moreover, increasing of TiO_2 contents from 10 to 20 wt% (double loading) led to the 1.2-fold increment of particle size. The radius of gyration (R_g) of rigid rod SSG molecule in an aqueous solution was found to be around 53-56 nm [26]. The average biopolymer rod diameter can

approximately to be $2R_g$ = 106-112 nm. Thus, nano-TiO$_2$ particle size (21 nm) is much smaller than polymer rod diameter value. This will cause a high bridging density even at the lowest NPs adding since individual SSG chains can physically connect to multiple TiO$_2$. This condition beside powerful adsorption strength (H-bonding and Ti coordination) propelled to strong polymer-nanoparticle bridging interactions.

When NPs content increased, the number and size of SSG-TiO$_2$ flocculate and clusters increased, and the bridging interactions were strengthened. Hence, a 3D percolated matrix-NPs network was gradually developed. These microstructures play the most decisive role in the control of physicochemical and rheo-mechanical properties of nanocomposite hydrogels. These observations were in accordance with those obtained for gelatin-TiO$_2$ [27], Poly(ethylene oxide)-SiO$_2$ [28], xanthan-ZnO and xanthan-CuO [29] dispersions. In contrast, Oliveira et al. [13] indicated that increasing the amount of SiO$_2$-NPs added to the locust bean gum (LBG) matrix increased the number of polymer-particle clusters, but not their average size.

Table 1

3.2. Zeta (ζ)-potential

Zeta (ζ)-potential reflects the effective charge of molecules in the dispersed system. The variation of ζ-potential of nanocomposite material can be used as an indicator of the adsorption extent and electrostatic attraction/repulsion between polar or charged ion components. ζ-potential is also a practical measurement for classification of stability of the multi-phase system via the DLVO (Derjagin-Landau-Verwey-Overbeek) surface steric force theory, which stated the more stable substance had higher ζ-potential magnitudes (near to ±30) [30]. The ζ-potential of 1% (w/w) nano-

TiO$_2$ and SSG solutions were approximate -12.7 and -53.1 mV, respectively, at neutral pH (Table 1), showed a weak and strong negative charge on the surface of TiO$_2$-NPs and SSG (anionic biomacromolecule), respectively. These values are expected, in accordance with the magnitudes in the literature [31,32] and suggested that SSG and TiO$_2$ can act as an electron donor and acceptor, respectively [33]. As shown in Table 1, the addition of TiO$_2$ in the low concentration (up to 5 wt%) into the SSG colloidal gel did not affect the electrokinetic behavior of nanocomposite hydrogel. The possible reason for this finding might be that SSG is a long chain molecule when compared with the nanospheres of TiO$_2$, especially at low contents. The SSG-TiO$_2$ flocculates were rapidly formed and the flocculates might be covered by SSG, resulting in an unaltered negatively charged surface of the flocculates, independent of the TiO$_2$ concentration. The negative values of the ζ-potential of SSG-based gel decreased significantly upon nano-TiO$_2$ loading ($\geq$ 10 wt%), demonstrated that the dispersant NPs gradually covered and bound to the surface of the SSG macromolecules. However, in the case of SSG-25TiO$_2$, the ζ-potential (-39.7 mV) is higher than the minimum value (-30 mV) which considered to a stable nanosuspension. The reduction of ζ-potential in the presence of TiO$_2$ at high concentration ($\geq$ 10 wt%) and the lowest surface charge magnitude of the highest TiO$_2$ fraction sample (SSG-25TiO$_2$) might be ascribed by the higher polymer-particle adsorption and interactions, created larger flocculated clusters having lower electrophoretic (electrokinetic) mobility with an increase in NPs fraction compared to small particles and flocculates, which can result in a decrease of ζ-potential [34]. It should also be noted that the increment in particle size led to a decrease of the specific surface area of the particles. Considering the number of the charged groups on particle surface commensurate with the specific surface area, the increase in particle size could lead to a decline in the surface charge and the ζ-

potential. This result was in good agreement with those reported for gelatin-nanoclay hydrogel [14].

3.3. Density

Density and its derivatives are essential intensive factors in fluid mechanics calculations and predicting the material thermodynamic properties and rheo-texture behavior. The density is directly proportional to the porosity (volume fraction, sizes, and their interconnection) of the hydrogel networks, which affected by composition and components interactions. Experimental values of SSG-based hydrogel density measurements shown in Table 1, presented with increasing TiO_2 mass fraction (0-25 wt%), the overall density of nanocomposite hydrogels shifted to higher values, as expected since the average density of the solid constituents of the SSG-TiO_2 composite is higher than pure SSG density. The upward trend of the density indicated the specific volumetric shrinkage of the SSG-based hydrogel components upon TiO_2 loading, which might be associated with the formation high-density inter and intramolecular agglomerate/aggregates microstructures due to the physicochemical interactions (H-bonding and chain entanglement) between the functional groups in SSG matrix and TiO_2-NPs. Beside, polyelectrolytes coil dimensions in SSG may be shrunk by long-range electrostatic attractions [6]. Furthermore, positively charged TiO_2 surface (-Ti^{4+}-O) can form bridges between acid groups. Most of these bridges are intramolecular links, therefore lead to a further diminishing of the volume occupied by the hydrogel. It should also be noted that two different behaviors were seen depending on nano-TiO_2 percentage. For C_{NPs} ≤ 15 wt%, density presented a slight dependence on solid content and increase from 1.47 in pure SSG to 1.50 g/ml for SSG-15TiO_2 was obtained, whereas for higher nanoparticle contents (>15 wt%), an abruptly increment in density with a very strong dependence on solid content could be

12

noted. Apart from the obvious effect of shrinkage, the role of nano-TiO_2 in increasing trend/order of density variations was not clear and no discussion has gone on it in the literature. However, similar results were observed for the swelling behavior of the polyacrylamide/alginate reinforced by different nanoparticles (SiO_2, Al_2O_3, and TiO_2) [20] and carrageenan-silver [35] hydrogels due to the extra attractive force between polymer chains and NPs and decrease in porosity of the hydrogel networks.

3.4. Surface tension

Surface tension often plays a significant role in nanocomposite solution stability, its application as a delivery system or predicting the evaporation rate in film or aerogel preparation. When TiO_2 was introduced to SSG gel, the surface energy of the gas-liquid interface gets affected because NPs induction changes at the molecular level through electrostatic interactions [36]. Surface tension decreased significantly at 5 wt% NPs in comparison with pure SSG (Table 1), demonstrated the presence of hydrophilic TiO_2-NPs might pull more liquid molecules down from the interface, towards the particle floating in the interior and created a less dense region, so that reduced the free energy of the new interface in the SSG-5TiO_2 nanohybrid hydrogel. This observation suggested that TiO_2-NPs can act as a surface-active additive like as nano-SiO_2 [37] at low levels (≤ 5 wt%). A similar result was previously reported by Chinnam et al. [38] using different spherical metal oxide NPs (TiO_2, Al_2O_3, and SiO_2) at concentrations below 6% (w/w) in propylene glycol-water nanofluid. Surface tension of SSG-TiO_2 nanocomposite increased significantly (64.0 mN/m) until $C_{NPs} = 10$ wt% and reduced to 60.6–61.6 mN/m at $C_{NPs} = 15$-25 wt%. It has been mentioned that enhance in surface tension and its irregular trend displayed at higher C_{NPs} could be related to the high viscosity of SSG-TiO_2 composite hydrogel at higher NPs contents, which made interfacial

measurement difficult by common techniques. In addition, the rise of the hydrogel density caused by the shrinkage presumably led to a settlement trend of the flocs, which affected the results of the surface tension measurement. This result was compatible with the results observed by Vafaei et al. [36] and Ranjbar et al. [39], which indicated that the surface tension of bismuth telluride (Bi_2Te_3), Tri Ethylene Glycol-Al_2O_3 and -MgO nanofluid diminished to a minimum magnitude and then increased again with the loading of more NPs. They adjudged that this type of behavior in surface tension to be an outcome of charged NPs assembly and accumulation at the liquid-gas interface.

3.5. Stress sweep

Amplitude stress sweep test was conducted prior to performing the frequency sweep, to ensure operation within the LVE region and characterize the stress dependence of the viscoelastic response. According to the stress sweep outcomes, the frequency sweep assessments were carried out under the constant stress of 0.1 Pa. Besides, the effects of TiO_2-NPs on rheological behavior pattern and some related parameters from stress sweep presented in Fig. 1 and Table 2. In all SSG-based hydrogels with raising stress, two distinct regions were distinguished, (a) LVE region where G' and G'' were approximately steady and parallel with $G'_{LVE} > G''_{LVE}$ (solid-like demeanor); and (b) n-LVE (nonlinear range) in which G' and G'' commenced to decrease. Generally, the magnitudes of G'_{LVE} and G''_{LVE} of the SSG-based hydrogels increased significantly ($P < 0.05$) upon TiO_2 addition (5-25 wt%), demonstrating the increase of system solidity (Table 2).

Figure 1

Table 2

The increment in G'_{LVE} is marginal at low filler loading (up to 5 wt%), slowly increases with augmenting C_{NPs} and becomes noticeable above 15 wt%. In contrast, the increment in G''_{LVE} of the nanocomposites due to the TiO_2 addition was already substantial at 5 wt%, which revealed that elastic and viscous elements were more affected by nano-TiO_2 at high and low contents, respectively. G^*_{LVE} which includes both viscoelastic moduli of a system showed an alike trend with G'_{LVE} and illustrated that the total structural strength of SSG-based nanocomposite rose with NPs incorporation due the reinforcing effect of the inclusions (primary particles and clusters) [40]. $Tan(\delta)_{LVE}$ was another assayed parameter which is defined as the ratio of loss to storage energy in the LVE range and stating the physical behavior of a system. All instances showed $0.1 < tan(\delta)_{LVE} > 1$, demonstrated the predominance of G' which is the typical response of weak gels. Except at 5 wt% TiO_2, $tan(\delta)_{LVE}$ of hydrogels decreased with the increase of C_{NPs} (Table 2). Nanocomposite containing 5 and 25 wt% TiO_2 had highest and lowest $tan(\delta)_{LVE}$, respectively, which can be explained by the enhanced contribution of the viscous and elastic components at lower and higher C_{NPs}.

Dynamic yield stress (τ_d) is defined as the limiting values of stress at the LVE range which caused the first non-linear microstructural changes. It depends on the molecular architecture in the matrix-particle structure and can be considered as the beginning point of the weakening of the gel strength. With the increase in C_{NPs} from zero to 25 wt%, the τ_d significantly decreased from 4.45 to 1.45 Pa (Table 2). This phenomenon is usually attributable to the stress-induced disruption of the fragile structural interactions among the network building units. This kind of demeanor was observed for LBG-SiO_2 solutions in the similar NPs concentration regime (0-20 wt%) [13]. They ascribed this behavior to the low ionization of the SiO_2-NPs or high ionic strength where the counter-ions can

shield the charges on the SiO_2 particles, especially for the systems with high C_{NPs}. Similar causes might apply for SSG-TiO_2 hydrogels. Meanwhile, the shorter lasting structure of SSG-TiO_2 than that of SSG alongside the stress axis may be due to the presence of powerful bonds in SSG-TiO_2 compared to pure SSG, which limited the chains mobility in the SSG-TiO_2 hydrogel, hence, the time needed to form new interactions to replace those ruined by the external stress. On the contrary, static yield stress (τ_s) of nanocomposite hydrogel increased significantly with the increase of TiO_2 fraction, except for 5 wt% (Table 2). These different results with opposite trends in τ_d and τ_s indicated the existence of two different kinds of crosslinked or other interactive microstructure in the system. T_d has demonstrated the value of stress for stopping a flowing test material (conversion from a viscoplastic to the solid behavior) which is related to more strong and insensitive construct to shear rate. On the other hand, the τ_s is related to the shear-sensitive microstructure which formed over a definite period when the sample is at rest state, thus it is the magnitude of stress required to get the test material starts to flow (transformation from solid to viscoplastic state). Moreover, the τ_s was greater than the τ_d at each C_{NPs} and the value of τ_d/τ_s ratio decreased as C_{NPs} increased because τ_s is an outcome of the combined structure [5]. These results suggested that with an increase in C_{NPs}, the shear-sensitive (τ_s) and shear-insensitive (τ_d) microstructure extent in SSG-based hydrogel enhanced and reduced, respectively. The opposite trend of τ_d with the viscoelastic moduli in the LVE range (G'_{LVE} and G''_{LVE}) suggested the formation of a more strong but fragile 3D temporary network microstructure upon C_{NPs} loading and supported the idea that interfacial slippage occurred in the higher filler composites. For all hydrogels, beyond the critical stress amplitude, the LVE range was utterly left and G' can cross G" (G'=G") (Fig. 1). At this point, the material collapses and the gel structure is irreversibly altered. The stress at crossover/flow point (τ_f) which illustrates the stress of viscoelastic to elastoviscous state transformation, considered as

a good indicator of resistance to flow. T_f for SSG-based hydrogels decreased as C_{NPs} increased up to 5 wt% but thereafter gained to the highest amount of 19.40 Pa at 20 wt%, showing slight inclination to flow of SSG-20TiO$_2$ nanocomposite (Table 2). At the flow point, viscoelastic moduli diminished rapidly, thus the corresponding modulus (G_f) indicates the system stiffness and behavior changes. G_f increased significantly from 13.64 to 15.21 Pa as a function of C_{NPs} (0-15 wt%) and remain constant at high C_{NPs} ($\geq$ 15 wt%), presented that the matrix-filler associations prevailed the effect of deformation force.

As the applied stress was increased, the gel body failure led to a sharp reduction in the G' and G" magnitudes. Failure strain or stress was distinguished as the strain/stress at which macroscopic rupture arise in the system. Failure properties are usually regarded as indicators of structural arrangement and an important part of a comprehensive evaluation of gel stability and load-bearing applications. Failure stress (τ_{Fr}) of plain SSG and SSG-15TiO$_2$ are shown in Fig. 2. SSG-based hydrogels exhibited characteristic increases in γ_{Fr} with C_{NPs} as follows. In the low C_{NPs} region (up to 5 wt%), γ_{Fr} and τ_{Fr} changed insignificantly. The early failure of hydrogels is reasonably due to the laxity of the gel systems, made them incapable to tolerate large external forces. Besides, a matrix carrying the highest stress, normally the shortest and weakest one in extension and linkage, respectively, failed first. Between 5 and 15 wt% TiO$_2$, γ_{Fr} and τ_{Fr} increased more rapidly with increasing C_{NPs}, and finally from 15 to 25 wt%, the value of γ_{Fr} and τ_{Fr} decreased considerably, but they were still much greater than that of the pure SSG hydrogel (Table 2). The precipitous increase in the range of 5-15 wt% TiO$_2$ may be related to the formation of the rigid microstructure. The reason for γ_{Fr} and τ_{Fr} reduction for C_{NPs} above 15 wt% is the increased brittleness, probably due to the presence of large-scale aggregated excessive TiO$_2$-NPs in the gel matrix, which could diminish the structural integrity of hydrogel and its persistence versus crack initiation, propagation,

and failure [41]. These results are in line with previous findings that addition of hectorite and SiO_2-NPs improves fractural properties of the polyacrylamide derivatives hydrogel/hybrid materials [42,43].

Figure 2

Spreadability is a crucial subjective textural attribute of semisolid and elastoplastic biomaterial which could be shown as index of ease and uniform casting process (in film, aerogel, and tissue engineered scaffold fabrication), coating and therapy applications (wound healing, skin care, and topical creams). The higher value of $\tan(\delta)_{s(n-LVE)}$ which illustrates the viscous/elastic components behaviors changes with stress at the n-LVE range, could be considered as an indicator of higher spreadability index (SI) of a system. The $\tan(\delta)_{s(n-LVE)}$ values became steeper (higher SI) by incorporation of TiO_2-NPs in the semisolid SSG matrix and reached a maximum of 2.03 for SSG-$20TiO_2$ sample (Table 2). This might be related to the decrease of SSG polymer mass fraction from 1 in pure SSG gel to 0.83 in SSG-$20TiO_2$ nanocomposite hydrogel. It is important to note that the SI gave similar trend with gumminess and inverse trend to the cohesiveness and dynamic yield stress.

3.5. Frequency sweep

Typical frequency (ω) dependence linear viscoelasticity of pure SSG and SSG-$20TiO_2$ over the range of 0.1-10 Hz at a fixed stress and temperature (0.1 Pa, 20°C) was shown in Fig. 3, respectively. In all SSG-based nanocomposite, the value of G' was almost independent of ω (plateau-like), higher than that of G''(ω) and without any cross point in the applied frequency, suggested the SSG-based systems were viscoelastic solid-like hydrogels.

18

Figure 3

The variation in $G'_{1\,Hz}$, $G''_{1\,Hz}$, $G^*_{1\,Hz}$, $\eta^*_{1\,Hz}$ and $\tan\delta_{1\,Hz}$ of SSG-based hydrogels were presented in Table 3 as a function of TiO$_2$-NPs concentration. It can be seen that increasing C_{NPs} from 5 to 20 wt% caused a prominent increase, from 34.9 to 59.1 Pa in $G'_{1\,Hz}$ of instances. Elastic behavior is related to the number of cross-links and bridges in the material [41] thus the higher $G'_{1\,Hz}$ magnitude was associated with tougher hydrogel (SSG-20TiO$_2$), which were in accordance with stress sweep findings (Table 2). However, the results demonstrated clearly that further addition of TiO$_2$ (up to 25 wt%) decreased $G'_{1\,Hz}$ to 51.3 Pa, illustrated softening of the hydrogels due to the incorporation of exceeded NPs.

Similar observations were recently reported on the effect of nano-TiO$_2$ in collagen or collagen/chitosan [41], poly(vinyl alcohol) [44] and chitin [45] hydrogels. They have found that above a certain NPs concentration, the rheo-mechanical properties of a polymer-TiO$_2$ hybrid have remarkably declined due to the existence of the coarser particles resulting from the aggregation of originally introduced nano-TiO$_2$. Presumably, a similar mechanism of TiO$_2$-NPs disjunction from the SSG matrix and creation of numerous loosened clusters which prevent the cross-linking process, resulting in worsening of rheological properties operated in these systems. $\text{Tan}\delta_{1\,Hz}$ of SSG-based hydrogels was in the range of 0.42-0.54, which indicated their weak biopolymer hydrogel construct. $G''_{1\,Hz}$, $G^*_{1\,Hz}$, and $\eta^*_{1\,Hz}$ showed a similar trend with $G'_{1\,Hz}$ at any SSG-TiO$_2$ ratio (Table 3). As C_{NPs} increased, $\eta^*_{1\,Hz}$ enhanced considerably, reflected that TiO$_2$ enhanced the strength of the biopolymeric matrix, probably as the NPs mediate chain interactions fabricated sizable domains of aggregated/self-associated SSG (refer to section 3.1). However, upon 25 wt%

TiO$_2$ loading, $\eta^*_{1\,Hz}$ decreased significantly, illustrated the high viscosity of the nanocomposite hydrogels was not a direct outcome of the particles size but was contributed to the strong propensity of particles to create clusters [40].

Figure 4

Complex viscosity (η^*) decreased almost linearly with the increment of frequency in all hydrogels (Fig. 4) revealed non-Newtonian shear-thinning behavior (pseudoplastic nature) of SSG-based hydrogels which revealed the presence of interlacing molecular interactions in the system. Shear-thinning demeanor may be due to the formation of the shear-induced alignment of the SSG-TiO$_2$ segments towards the flow direction. Besides, at high frequency the period time is not adequate to rebuild broken intra- and intermolecular linkage, disentanglement or molecular alignment of long-chain polymers, and subsequently, the downtrend in η^* occurred [5]. The slope of the η^*-frequency curves (η^*_s) of pure SSG was -0.82. It increased after TiO$_2$ loading, approved that the elasticity of the samples was positively affected by the addition of TiO$_2$-NPs. η^*_s of SSG-based hydrogels in the range from -0.80 to -0.89, which were remarkably higher than the highest magnitude of -0.76 which considered for weak polysaccharide gel, formed by overlapping and entangled flexible random coil chains.

Table 3

Table 4

Power law model (Eqs. (1), (2) and (3)) delineated adequately the frequency dependence of the G',

20

G" and G^* moduli for all SSG-based instances. It was found that all hydrogels exhibited solid-like elastic behavior because the slopes ($n' = 0.11$-0.28 and $n'' = 0.26$-0.58) were much lower than values suggested for a simple Maxwellian system ($G' \propto \omega^2$ and $G'' \propto \omega$), and K' magnitudes much larger than those of K''. In addition, n' and n'' values (frequency dependence) decreased and K' and K'' increased with the rise in C_{NPs} (up to 20 wt%), pointed out that the polymer relaxation, chain reputation, and 3D network became slower, more restrained and stronger, respectively (Table 4). With further increment in TiO_2 to 25 wt%, the rigidity of continuous phase deteriorated (enhancement of n' and n'' and reduction of K' values). Since the simply reinforcing effect would give an increase in viscoelastic moduli without a change in the frequency dependence (n' and n''), obtained results illustrated a structural modification of the nanocomposites with the TiO_2 load [46]. The strength and the number of conceivable interactions in the SSG-TiO_2 3D network were specified by using the material stiffness parameter (A_α) and the order of relaxation function (α) (Table 4). With increasing TiO_2 fraction, the values of A_α raised except for SSG-25TiO_2 which showed lower stiffness than SSG-20TiO_2 indicated the increase in the polymer-polymer and polymer-particle bridging or cross-linking (network strength) with C_{NPs}. The origin of enhancing in stiffness might be pertinent to the creation of large-scale microstructures, heterogeneities and possibly compacted SSG-TiO_2 segments that act as elastic springs to augment the 3D network structure. In addition, α abated with C_{NPs} increment. Lower magnitude of α related to a higher number of interactions, greater network extension and shear thinning behavior in SAOS [5].

3.4. Large deformation properties

Most of the practical application features of hydrogels, such as handling, shaping and casting (for scaffold tissue, film and aerogel fabrication) are closely related to the large deformation and

fracture characteristics of gels. Therefore, the internal network properties of SSG-based hydrogels and reinforcement effect of nano-TiO$_2$ at large deformation values were studied with the texture profile analysis (TPA) test. The important textural properties were determined from the resultant force-time curves (Table 5). All hydrogels indicated a rapid non-linear increase in the force over a short time as the probe propelled into the samples, even though the initial slope was dissimilar for different hydrogels (data not shown), demonstrated the formation of elastic and stiff systems relying on the SSG-TiO$_2$ ratio. In addition, the non-linear correlation of force and corresponding deformation supported the non-Gaussian nature of the SSG-based network distribution over the whole range of deflection, manifested in a non-linear relationship between force and distance of polymer crosslinks and bridges connections. With an increase in C$_{NPs}$ from zero to 15 wt%, the hardness increased prominently from 255 g to 325 g. Nevertheless, incorporation of more TiO$_2$-NPs up to 20 wt% led to a slight reduction in hardness (307 g) and afterward, it sharply decreased to the lowest value of 246 g in SSG-25TiO$_2$. An increment in hardness of SSG-TiO$_2$ hydrogels might be exhibited the creation of clusters of ordered microstructure along the polysaccharide chains upon TiO$_2$ addition, which subsequently led to aggregation of these junction zones and formation a more rigid and compact 3D percolated network. Such observations were similarly made in the tamarind seed gum-nanofibrillated cellulose [3] and alginate [47,48] hydrogels. They ascribed this behavior by strain-stiffening (-hardening) effect which is a rather general phenomenon for biopolymeric-based gel [49]. Several possible scenarios such as high stretchability and loose consistency [3], deformation of rod-like junction zone [47], structure densification and highly crosslinked polymer systems [48] have been proposed to explain the strain-stiffening phenomenon. According to aforementioned observations, strain-stiffening became more notable as C$_{NPs}$ increased up to 15 wt%, but thereafter it diminished. The relative

and abruptly decrease in hardness and strain-stiffening at C_{NPs} = 20 and 25 wt%, respectively, presumably be attributed to the heterogeneous microstructure resulting from more aggregation of TiO_2, as mentioned earlier.

Table 5

Cohesiveness is an index of internal structure strength and its resistance to breaking down. When the C_{NPs} increased from 0 to 15 wt%, the cohesiveness value decreased from 0.68 to 0.56, probably due to the inhomogeneous embedding of TiO_2-NPs, and consequently partially phase separation in the system. On the other hand, when C_{NPs} increased to 25 wt%, cohesiveness rose and attained 0.62 (Table 5). This behavior was also observed in gelatin- [50], guar- and tamarind seed gum-nanofiber cellulose [3] hydrogels and pointed out that the internal structure of nanocomposite gel became more brittle (facile to break) by the initial compression, with increasing C_{NPs}. The adhesiveness is an interfacial property which demonstrates the force of holding dissimilar particles/surfaces together for extended periods of time. Adhesion characteristics can undoubtedly have a significant impact on energy consumption in fluid transportation and cooling/heating process of operations via boundary layer effect. The extent of adhesion depends on various factors including the size, flexibility, conformation and other physicochemical properties of the polymer and the environment in which it resided in. Adhesive strength has been shown a positive correlation with polymer molecular weight and its solution viscosity [51]. As C_{NPs} increased up to 5 wt%, adhesion energy reduced, on the contrary, samples with higher C_{NPs} (10-15 wt%) had a more significant trend of hydrogel adhesion (stickiness) on the surface. Adhesiveness decreased with the increased loading of TiO_2 content (20 and 25 wt%) into the SSG matrix, might be due to high

cohesive bond strength in these hydrogels that prevents the formation of adhesive interactions [52]. These results were in accordance with that reported for poly(ethylene glycol)-SiO_2 nanocomposite hydrogel stickiness [53] and demonstrated that the formation and strength of adhesive interactions were mainly governed by NPs filling, composition and network homo-heterogeneity of the hydrogel matrix. Six general theories have been adapted to describe the fundamental mechanisms involved in biological macromolecules stickiness [54]. We believe that the fracture theory which assumed that the failure of the adhesive bond occurs at the weakest interface is appropriately explained the detachment force in the semi-rigid SSG-based hydrogel. In this theory, the adhesive strength and work of failure have a direct relation with Young's modulus of elasticity and molecular weight of the network strands, respectively [55].

Springiness which sometimes referred as gel elastic recovery or rubberiness shows the physically springs back of a sample after the first compression. Gumminess is the denseness that persists throughout deformation or the energy required to disintegrate a semi-solid material and used to describe its viscous properties [56]. Similar to other textural characteristics, two different behaviors were observed depending on TiO_2 concentration (Table 5). For $C_{NPs} \leq 10$ wt%, an increase of springiness and gumminess could be noted, whereas for $C_{NPs} > 10$ wt%, a diminution in these factors was acquired. This observation reflected that at low C_{NPs} (≤ 10 wt%), the structure of SSG-TiO_2 gel was broken into few massive pieces during the first TPA compression whilst at $C_{NPs} > 10$ wt%, less springy texture resulted from the hydrogel breaking into many small pieces [57]. The initial tangent modulus or apparent modulus of elasticity (E_a) is a measure of the degree of the material stiffness at low deformation level. As expected, with increasing C_{NPs} from 0 to 15 and 25 wt%, the values of E_a first increased from 106.4 to 177.6 g/s, and then decreased to 103.9 g/s (SSG-25TiO_2), revealed that TiO_2-NPs act as physical crosslinking reagents [58] and created

24

a stiffer microstructure at low TiO_2 levels (≤ 15 wt%). The E_a reduction with higher C_{NPs} can be attributed to the degradation of the integrity of the hydrogels network structure as discussed earlier.

4. Conclusions

In this study, the physicochemical and rheo-mechanical characteristics of new environmental friendly TiO_2-reinforced, SSG-based hydrogels were investigated. Incorporation of TiO_2-NPs significantly decreased the zeta potential, and enhanced density and particle size of SSG-TiO_2 hydrogels besides, severely changed their surface tension. Local secondary microstructure (soft flocks and hard clusters) formation and percolated 3D network, depending on their number and strength (as a consequence of the chain entanglement, polymer-particle, and interparticle possibly interactions), lead to gel structural modification evidenced by a gradual increase in viscoelastic moduli and decrease in their frequency dependency. Non-linear viscoelastic region data indicated the incorporation of nano-TiO_2 increased the spreadability index of NFS, which is a favor in skin care creams and coating substances. Large deformation mechanical analysis also confirmed that the addition of TiO_2-NPs up to a critical level (15 wt%) caused hydrogels to be more hard, adhesive, springy and less cohesive. However, these incremental effects diminished with the NPs load beyond 15 wt%. The knowledge of the rheo-mechanical characteristics of hydrogels systems is crucial to handle the NFS casting/application on support or use as spreadable biomaterials. Taking into account all data demonstrated, it can be declared that developed SSG-15TiO_2 nanohybrid hydrogel is a promising candidate for bio-based composites applications where the tunable textural features and augmented structures are favorable.

References

[1]   K. Haraguchi, H. Li, Mechanical properties and structure of polymer-clay nanocomposite gels with high clay content, Macromolecules. 39 (2006) 1898–1905.

[2]   F. Ullah, M.B.H. Othman, F. Javed, Z. Ahmad, H.M. Akil, Classification, processing and application of hydrogels: A review, Mater. Sci. Eng. C. 57 (2015) 414–433.

[3]   A. Ghafar, K. Parikka, T. Sontag-Strohm, M. Österberg, M. Tenkanen, K.S. Mikkonen, Strengthening effect of nanofibrillated cellulose is dependent on enzymatically oxidized polysaccharide gel matrices, Eur. Polym. J. 71 (2015) 171–184.

[4]   T. dos Santos, R. Hernández, N. Rescignano, L. Boff, H. Reginatto, C. Simões, A. de Campos, C. Mijangos, Nanocomposite chitosan hydrogels based on PLGA nanoparticles as potential biomedical materials, Eur. Polym. J. 99 (2018) 456–463.

[5]   S.M.A. Razavi, A. Alghooneh, F. Behrouzian, Influence of temperature on sage seed gum (*Salvia macrosiphon*) rheology in dilute and concentrated regimes, J. Dispers. Sci. Technol. (2017) 1–14.

[6]   F. Behrouzian, S.M.A. Razavi, A. Alghooneh, Evaluation of interactions of biopolymers using dynamic rheological measurements: Effect of temperature and blend ratios, J. Appl. Polym. Sci. 134 (2017).

[7]   P. Li, N.H. Kim, D. Hui, K.Y. Rhee, J.H. Lee, Improved mechanical and swelling behavior of the composite hydrogels prepared by ionic monomer and acid-activated Laponite, Appl. Clay Sci. 46 (2009) 414–417.

[8]   S. Ahmadzadeh, A. Nasirpour, J. Keramat, S. Desobry, Effect of surface-modified montmorillonite on viscosity and gelation behavior of cellulose/NaOH solution, Cellulose.

22 (2015) 1829–1839.

[9]   Z. Zare-Akbari, H. Farhadnejad, B. Furughi-Nia, S. Abedin, M. Yadollahi, M. Khorsand-Ghayeni, PH-sensitive bionanocomposite hydrogel beads based on carboxymethyl cellulose/ZnO nanoparticle as drug carrier, Int. J. Biol. Macromol. 93 (2016) 1317–1327.

[10]   S.A. Oleyaei, S.M.A. Razavi, K.S. Mikkonen, Novel nanobiocomposite hydrogels based on sage seed gum-Laponite: Physico-chemical and rheological characterization, Carbohydr. Polym. 192 (2018) 282–290.

[11]   R. Lapasin, M. Abrami, M. Grassi, U. Sebenik, U. Šebenik, Rheology of Laponite-scleroglucan hydrogels, Carbohydr. Polym. 168 (2017) 290–300.

[12]   J.L. Dávila, M.A. d'Ávila, Laponite as a rheology modifier of alginate solutions: Physical gelation and aging evolution, Carbohydr. Polym. 157 (2017) 1–8.

[13]   F. Oliveira, S.R. Monteiro, A. Barros-Timmons, J.A. Lopes-da-Silva, Weak-gel formation in dispersions of silica particles in a matrix of a non-ionic polysaccharide: Structure and rheological characterization, Carbohydr. Polym. 82 (2010) 1219–1227.

[14]   F. Karimi, N. Taheri, R. Namivandi, Fish gelatin/Laponite biohybrid elastic coacervates: A complexation kinetics-structure relationship study, Int. J. Biol. Macromol. 61 (2013) 102–113.

[15]   J.R.M. Kennedy, K.E. Kent, J.R. Brown, Rheology of dispersions of xanthan gum, locust bean gum and mixed biopolymer gel with silicon dioxide nanoparticles, Mater. Sci. Eng. C. 48 (2015) 347–353.

[16]   B. Ghanbarzadeh, S.A. Oleyaei, H. Almasi, Nanostructured Materials Utilized in Biopolymer-based Plastics for Food Packaging Applications, Crit. Rev. Food Sci. Nutr. 55 (2015) 1699–1723.

[17] S.A. Oleyaei, H. Almasi, B. Ghanbarzadeh, A.A. Moayedi, Synergistic reinforcing effect of TiO$_2$ and montmorillonite on potato starch nanocomposite films: Thermal, mechanical and barrier properties, Carbohydr. Polym. 152 (2016) 253–262.

[18] S.A. Oleyaei, Y. Zahedi, B. Ghanbarzadeh, A.A. Moayedi, Modification of physicochemical and thermal properties of starch films by incorporation of TiO$_2$ nanoparticles, Int. J. Biol. Macromol. 89 (2016) 256–264.

[19] M. Nešić, J. Žakula, L. Korićanac, M. Stepić, M. Radoičić, I. Popović, Z. Šaponjić, M. Petković, Light controlled metallo-drug delivery system based on the TiO$_2$-nanoparticles and Ru-complex, J. Photochem. Photobiol. A Chem. 347 (2017) 55–66.

[20] Y. Zhai, H. Duan, X. Meng, K. Cai, Y. Liu, L. Lucia, Reinforcement effects of inorganic nanoparticles for double-network hydrogels, Macromol. Mater. Eng. 300 (2015) 1290–1299.

[21] R. Shu, Y. Gan, H. Lv, D. Tan, Preparation and rheological behavior of ethylene glycol-based TiO2 nanofluids, Colloids Surfaces A Physicochem. Eng. Asp. 509 (2016) 86–90.

[22] A. Shakouri, H. Ahmadi, M. Hojjat, S. Zeinali, Effect of TiO$_2$ Nanoparticle on Rheological Behavior of Poly(vinyl alcohol) Solution, J. Vinyl Addit. Technol. 23 (2017) 234–240.

[23] A. Bostan, S. Razavi, R. Farhoosh, Optimization of hydrocolloid extraction from wild sage seed (*Salvia macrosiphon*) using response surface, Int. J. Food Prop. 13 (2010) 1380–1392.

[24] C. Friedrich, L. Heymann, Extension of a model for crosslinking polymer at the gel point, J. Rheol. 32 (1988) 235–241.

[25] S. Naji, S.M.A. Razavi, Functional and textural characteristics of cress seed (*Lepidium sativum*) gum and xanthan gum: Effect of refrigeration condition, Food Biosci. 5 (2014) 1-8.

[26] S.M.A. Razavi, S.W. Cui, Q. Guo, H. Ding, Some physicochemical properties of sage (*Salvia macrosiphon*) seed gum, Food Hydrocoll. 35 (2014) 453–462.

[27] Q. He, Y. Zhang, X. Cai, S. Wang, Fabrication of gelatin-TiO_2 nanocomposite film and its structural, antibacterial and physical properties, Int. J. Biol. Macromol. 84 (2016) 153–160.

[28] Q. Zhang, L.A. Archer, Optical polarimetry and mechanical rheometry of poly (ethylene oxide)-silica dispersions, Macromolecules. 37 (2004) 1928–1936.

[29] S. Ponmani, J. Karen, M. William, R. Samuel, R. Nagarajan, J.S. Sangwai, Colloids and Surfaces A : Physicochemical and engineering aspects formation and characterization of thermal and electrical properties of CuO and ZnO nanofluids in xanthan gum, Colloids Surface A Physicochem. Eng. Asp. 443 (2014) 37–43.

[30] T. Coviello, A.M. Trotta, C. Marianecci, M. Carafa, L. Di Marzio, F. Rinaldi, C. Di Meo, F. Alhaique, P. Matricardi, Gel-embedded niosomes: Preparation, characterization and release studies of a new system for topical drug delivery, Colloids Surfaces B Biointerfaces. 125 (2015) 291–299.

[31] H. Mohammadzadeh, A. Koocheki, R. Kadkhodaee, S.M.A. Razavi, Physical and flow properties of d-limonene-in-water emulsions stabilized with whey protein concentrate and wild sage (*Salvia macrosiphon*) seed gum, Food Res. Int. 53 (2013) 312–318.

[32] M. Hashimoto, H. Takadama, M. Mizuno, T. Kokubo, Mechanical properties and apatite forming ability of TiO_2 nanoparticles/high density polyethylene composite: Effect of filler content, J. Mater. Sci. Mater. Med. 18 (2007) 661–668.

[33] J.J. Zhou, S.Y. Wang, S. Gunasekaran, Preparation and characterization of whey protein film incorporated with TiO_2 nanoparticles, J. Food Sci. 74 (2009) 50–56.

[34] J. Wang, G. Liu, L. Wang, C. Li, J. Xu, D. Sun, Synergistic stabilization of emulsions by

poly(oxypropylene)diamine and Laponite particles, Colloids Surfaces A Physicochem. Eng. Asp. 353 (2010) 117–124.

[35] S. Azizi, R. Mohamad, R. Abdul Rahim, R. Mohammadinejad, A. Bin Ariff, Hydrogel beads bio-nanocomposite based on Kappa-carrageenan and green synthesized silver nanoparticles for biomedical applications, Int. J. Biol. Macromol. 104 (2017) 423–431.

[36] S. Vafaei, A. Purkayastha, A. Jain, G. Ramanath, T. Borca-Tasciuc, The effect of nanoparticles on the liquid-gas surface tension of Bi_2Te_3 nanofluids, Nanotechnology. 20 (2009) 185702.

[37] B.P. Binks, A. Desforges, D.G. Duff, Synergistic stabilization of emulsions by a mixture of surface-active nanoparticles and surfactant, Langmuir. 23 (2007) 1098–1106.

[38] J. Chinnam, D.K. Das, R.S. Vajjha, J.R. Satti, Measurements of the surface tension of nanofluids and development of a new correlation, Int. J. Therm. Sci. 98 (2015) 68–80.

[39] H. Ranjbar, M.R. Khosravi-Nikou, A. Safiri, S. Bovard, A. Khazaei, Experimental and theoretical investigation on Nano-fluid surface tension, J. Nat. Gas Sci. Eng. 27 (2015) 1806–1813.

[40] M.A. Osman, A. Atallah, Effect of the particle size on the viscoelastic properties of filled polyethylene, Polymer. 47 (2006) 2357–2368.

[41] K. Zazakowny, J. Lewandowska-Łańcucka, J. Mastalska-Popławska, K. Kamiński, A. Kusior, M. Radecka, M. Nowakowska, Biopolymeric hydrogels-nanostructured TiO_2 hybrid materials as potential injectable scaffolds for bone regeneration, Colloids Surfaces B Biointerfaces. 148 (2016) 607–614.

[42] Q. Wang, R. Hou, Y. Cheng, J. Fu, Super-tough double-network hydrogels reinforced by covalently compositing with silica-nanoparticles, Soft Matter. 8 (2012) 6048–6056.

[43]   H.J. Li, K. Haraguchi, Mechanical and swelling/de-swelling properties of nanocomposite gel with high clay content, Polym. Prepr. Japan. 55 (2006) 1898–1905.

[44]   G.U. Badranova, P.M. Gotovtsev, Y. V. Zubavichus, I.A. Staroselskiy, A.L. Vasiliev, I.N. Trunkin, M. V. Fedorov, Biopolymer-based hydrogels for encapsulation of photocatalytic TiO$_2$ nanoparticles prepared by the freezing/thawing method, J. Mol. Liq. 223 (2016) 16–20.

[45]   M.L. Peralta Ramos, J.A. González, S.G. Albornoz, C.J. Pérez, M.E. Villanueva, S.A. Giorgieri, G.J. Copello, Chitin hydrogel reinforced with TiO2 nanoparticles as an arsenic sorbent, Chem. Eng. J. 285 (2016) 581–587.

[46]   G.A. Valencia, I.C.F. Moraes, L.H.G. Hilliou, R.V. Lourenço, P.J.D.A. Sobral, Nanocomposite-forming solutions based on cassava starch and laponite: Viscoelastic and rheological characterization, J. Food Eng. 166 (2015) 174–181.

[47]   J. Zhang, C.R. Daubert, E. Allen Foegeding, A proposed strain-hardening mechanism for alginate gels, J. Food Eng. 80 (2007) 157–165.

[48]   M. Mancini, M. Moresi, R. Rancini, Mechanical properties of alginate gels: Empirical characterisation, J. Food Eng. 39 (1999) 369–378.

[49]   C. Michon, C. Chapuis, V. Langendorff, P. Boulenguer, G. Cuvelier, Strain-hardening properties of physical weak gels of biopolymers, Food Hydrocoll. 18 (2004) 999–1005.

[50]   W. Wang, X. Zhang, A. Teng, A. Liu, Mechanical reinforcement of gelatin hydrogel with nanofiber cellulose as a function of percolation concentration, Int. J. Biol. Macromol. 103 (2017) 226–233.

[51]   S.L. Cook, S.P. Bull, L. Methven, J.K. Parker, V. V. Khutoryanskiy, Mucoadhesion: A food perspective, Food Hydrocoll. 72 (2017) 281–296.

[52] D.S. Jones, A.D. Woolfson, A.F. Brown, Textural, viscoelastic and mucoadhesive properties of pharmaceutical gels composed of cellulose polymers, Int. J. Pharm. 151 (1997) 223–233.

[53] A.K. Gaharwar, C.P. Rivera, C.J. Wu, G. Schmidt, Transparent, elastomeric and tough hydrogels from poly(ethylene glycol) and silicate nanoparticles, Acta Biomater. 7 (2011) 4139–4148.

[54] B. Boddupalli, Z.. Mohammed, R. Nath, D. Banji, Mucoadhesive drug delivery system: An overview, J. Adv. Pharm. Technol. Res. 1 (2010) 381–387.

[55] R.B. Gandhi, J.R. Robinson, Oral cavity as a site for bioadhesive drug-delivery, Adv. Drug Deliv. Rev. 13 (1994) 43–74.

[56] M.C. Bourne, Food texture and viscosity: Concept and measurement, 2nd ed., Academic Press, New York, 2002.

[57] M.H. Lau, J. Tang, a T. Paulson, Texture profile and turbidity of gellan/gelatin mixed gels, Food Res. Int. 33 (2000) 665–671.

[58] D. Wu, J. Xu, Y. Chen, M. Yi, Q. Wang, Gum Arabic: A promising candidate for the construction of physical hydrogels exhibiting highly stretchable, self-healing and tensility reinforcing performances, Carbohydr. Polym. 181 (2018) 167–174.

Figure captions

Fig. 1. Changes of G' (filled symbols) and G" (open symbols) in stress sweep of SSG (a), SSG-5TiO$_2$ (b), SSG-10TiO$_2$ (c), SSG-15TiO$_2$ (d), SSG-20TiO$_2$ (e) and SSG-25TiO$_2$ (f) nanohybrid hydrogels (f = 1 Hz and T= 20℃).

Fig. 2. The Effect of increasing stress amplitude on elastic stress (G'.γ) of pure SSG and TiO$_2$ reinforced SSG-based nanohybrid hydrogels.

Fig. 3. Frequency sweeps of G' (filled symbols) and G" (open symbols) for SSG (a), SSG-5TiO$_2$ (b), SSG-10TiO$_2$ (c), SSG-15TiO$_2$ (d), SSG-20TiO$_2$ (e) and SSG-25TiO$_2$ (f) nanohybrid hydrogels at LVE region (τ = 0.1 Pa) and T = 20 ℃.

Fig. 4. The effect of frequency on complex viscosity (η^*) of pure SSG and TiO$_2$ reinforced SSG-based nanohybrid hydrogels at τ = 0.1 Pa and T = 20 ℃.

Table 1. Zeta potential, particle size, surface tension and density of sage seed gum dispersion (1%) and SSG-TiO_2 nanocomposite hydrogels at 25℃.

Samples	Particle size (nm)	Zeta potential (mV)	Density (g/ml)	Surface tension (mN/m)
TiO_2-NPs	21 ± 2.0^a	-12.7 ± 1.3^e	-	-
SSG	277.6 ± 40.3^b	-53.1 ± 0.4^a	1.47 ± 0.01^a	62.2 ± 0.2^d
SSG-5TiO_2	499.7 ± 59.2^c	-54.3 ± 1.0^a	1.45 ± 0.03^a	58.2 ± 0.1^a
SSG-10TiO_2	764.9 ± 52.8^d	-48.5 ± 1.1^b	1.49 ± 0.01^b	64.0 ± 0.2^e
SSG-15TiO_2	889.4 ± 46.0^e	-47.9 ± 0.3^b	1.50 ± 0.02^b	61.6 ± 0.2^c
SSG-20TiO_2	$949.6\pm92.4^{e,f}$	-43.3 ± 0.6^c	1.91 ± 0.04^c	60.6 ± 0.2^b
SSG-25TiO_2	1009.1 ± 25.7^f	-39.7 ± 1.5^d	2.19 ± 0.02^d	61.5 ± 0.3^c

Different letters indicate significant differences between samples at P < 0.05 by Duncan test.

Table 2. Storage modulus (G'$_{LVE}$), Loss modulus (G"$_{LVE}$), complex modulus (G$^{*}_{LVE}$), loss-tangent (tan(δ)$_{LVE}$), dynamic yield stress (τ_d) and static yield stress (τ_s) in the linear viscoelastic region, flow-point stress (τ_f) with corresponding modulus (G$_f$), slope of the loss tangent at n-LVE range (Tan(δ)$_{s(n-LVE)}$), failure stress (τ_{Fr}) and failure strain (γ_{Fr}) for 1% dispersion of SSG-based hydrogels (f = 1 Hz and T = 20℃).

Parameters/Samples	SSG	SSG-5TiO$_2$	SSG-10TiO$_2$	SSG-15TiO$_2$	SSG-20TiO$_2$	SSG-25TiO$_2$
G'$_{LVE}$ (Pa)	39.83±1.2[a]	41.91±1.6[b]	45.12±0.9[c]	50.56±3.1[d]	54.39±1.5[e]	55.28±2.2[e]
G"$_{LVE}$ (Pa)	16.77±0.6[a]	20.66±0.2[c]	19.45±0.4 [b]	20.41±0.3[c]	21.73±0.5[d]	21.62±0.4[d]
G$^{*}_{LVE}$(Pa)	43.21±1.0[a]	46.72±1.2[b]	49.13±1.0[c]	54.52±1.3[d]	58.57±1.1[e]	59.35±0.9[e]
Tan(δ)$_{LVE}$	0.42±0.0[c]	0.49±0.0[a]	0.43±0.0[b]	0.40±0.0[d]	0.40±0.0[d]	0.39±0.0[d]
τ_d (Pa)	4.45±0.2[a]	4.57±0.2[a]	3.12±0.3[b]	2.13±0.2[c]	1.50±0.1[d]	1.45±0.1[d]
τ_s (Pa)	6.27±0.2[b]	5.89±0.1[a]	6.79±0.0[c]	6.92±0.1[c,d]	7.02±0.2[d]	7.99±0.1[e]
τ_f (Pa)	18.82±0.4[d]	16.60±0.1[a]	17.55±0.3[b]	19.08±0.2[d]	19.40±0.1[e]	18.24±0.2[c]
G$_f$ (Pa)	13.64±0.1[a]	13.67±0.2[a]	13.49±0.1[a]	15.21±0.3[b]	15.49±0.2[b]	15.45±0.3[b]
γ_{Fr} (%)	92.29±2.8[a]	91.15±2.2[a]	150.73±3.4[c]	159.92±3.1[d]	144.02±1.9[c]	109.48±3.7[b]
τ_{Fr} (Pa)	24.13±0.7[a]	24.58±0.2[a,b]	26.51±0.3[c]	27.30±0.1[d]	28.02±0.4[d]	25.51±0.2[b]
Tan(δ)$_{s(n-LVE)}$	0.41±0.0[a]	0.44±0.1[a]	0.64±0.0[b]	1.51±0.1[c]	2.03±0.1[d]	1.48±0.0[c]

Means followed by the different letters in the same rows are significantly different at P < 0.05 by Duncan test.

Table 3. Storage modulus (G'), viscous modulus (G"), loss-tangent (tanδ), complex modulus (G*), complex viscosity (η*) at f = 1 Hz, slope of complex viscosity (η$^*_s$) foe 1% dispersion of sage seed gum (SSG) and SSG-TiO$_2$ hydrogels at τ = 0.1 Pa and T = 20 ℃.

Parameters/Samples	SSG	SSG-5TiO$_2$	SSG-10TiO$_2$	SSG-15TiO$_2$	SSG-20TiO$_2$	SSG-25TiO$_2$
G'$_{1\,Hz}$ (Pa)	35.9±2.1^a	34.9±2.1^a	43.5±1.5^b	45.5±1.0^b	59.1±1.6^c	51.3±2.1^d
G"$_{1\,Hz}$ (Pa)	15.4±1.2^a	19.0±1.0^b	18.9±0.1^b	23.6±0.4^c	27.4±1.2^d	23.4±0.8^c
Tanδ$_{1\,Hz}$	0.42±0.1^a	0.54±0.0^d	0.43±0.1^b	0.52±0.1^d	0.46±0.0^c	0.45±0.1^c
G$^*_{1\,Hz}$ (Pa)	39.1±1.9^a	39.7±1.1^a	47.4±1.3^b	51.2±1.6^c	65.1±2.0^e	56.4±0.9^d
η$^*_{1\,Hz}$ (Pa.s)	6.2±0.2^a	6.3±0.3^a	7.5±0.1^b	8.2±0.2^c	10.4±0.3^e	8.9±0.2^d
η$^*_s$	-0.82±0.0^a	-0.80±0.0^a	-0.86±0.0^c	-0.84±0.0^b	-0.89±0.0^d	-0.89±0.0^d

Means followed by the different letters in the same rows are significantly different at P < 0.05 by Duncan test.

Table 4. Frequency dependence of the elastic and viscose moduli, the Friedrich-Heymann model parameters and the subtraction of average G' from G" for 1% dispersion of sage seed gum (SSG) and SSG-TiO$_2$ hydrogels ($\tau = 0.1$ Pa, T = 20°C).

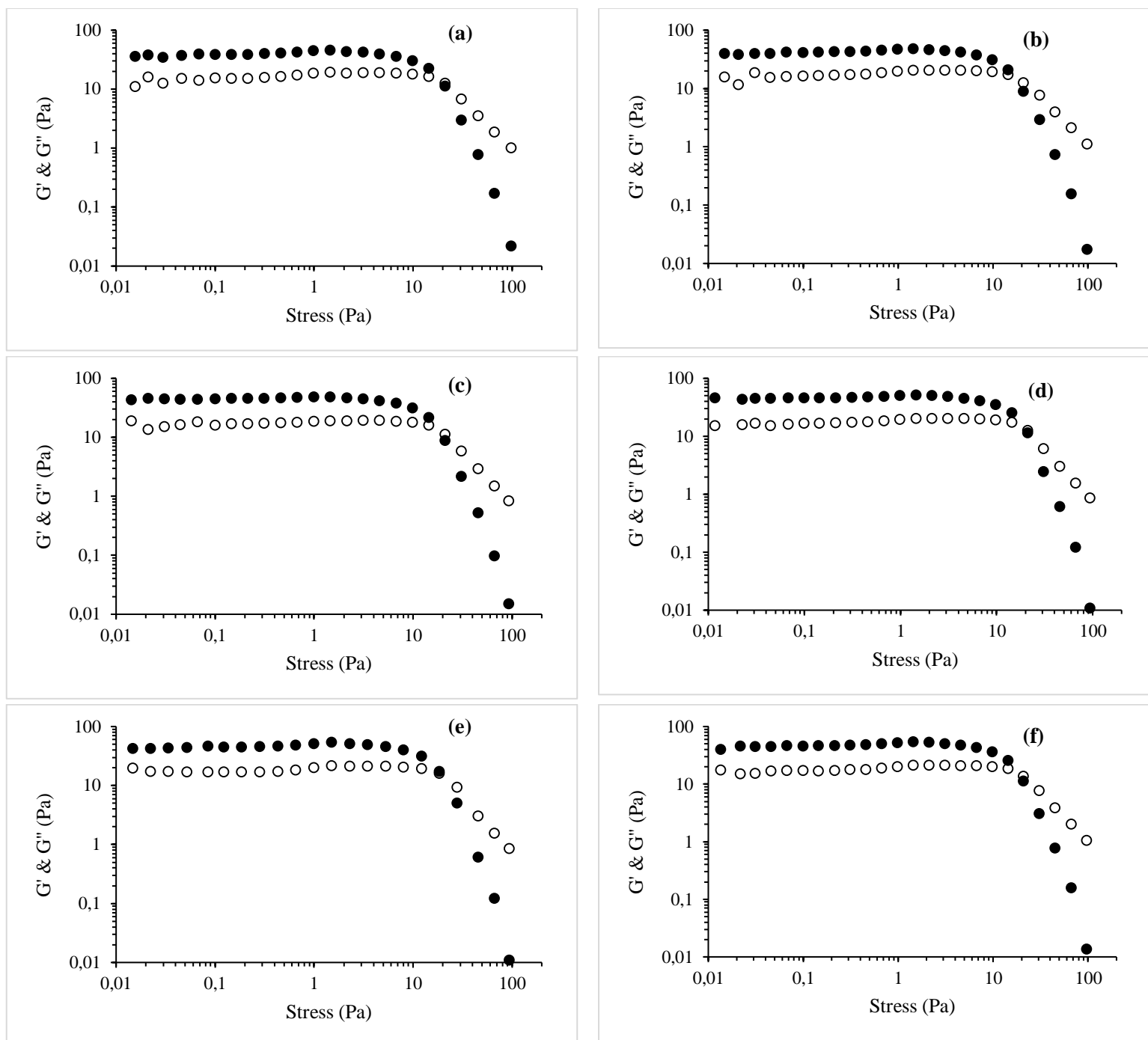| Samples	$G' = K' \times (\omega)^{n'}$			$G'' = K'' \times (\omega)^{n''}$			$G^* = A_\alpha \times (\omega)^\alpha$		
	K' (Pa)	n' (-)	R^2	K'' (Pa)	n'' (-)	R^2	A_α (Pa.rad$^{-\alpha}$.s$^\alpha$)	α (-)	R^2
SSG	27.83±0.5^a	0.28±0.0^a	0.94	5.58±0.3^b	0.52±0.0^b	0.96	28.69±1.5^a	0.29±0.0^a	0.98
SSG-5TiO$_2$	27.47±0.2^a	0.27±0.0^a	0.96	5.30±0.1^a	0.40±0.0^c	0.90	28.04±1.3^a	0.28±0.0^a	0.97
SSG-10TiO$_2$	32.55±0.3^b	0.18±0.0^b	0.98	7.69±0.4^d	0.39±0.0^c	0.92	34.70±2.0^b	0.24±0.0^b	0.95
SSG-15TiO$_2$	37.91±0.6^c	0.16±0.0^c	0.99	10.23±0.3^e	0.26±0.0^e	0.94	39.36±0.9^d	0.17±0.0^c	0.96
SSG-20TiO$_2$	46.69±0.5^d	0.11±0.0^d	0.96	16.84±0.6^f	0.36±0.0^d	0.96	50.46±1.3^e	0.17±0.0^c	0.98
SSG-25TiO$_2$	37.02±0.4^c	0.16±0.0^c	0.96	6.36±0.2^c	0.58±0.0^a	0.96	37.12±1.4^c	0.16±0.0^c	0.96

Means followed by the different letters in the same columns are significantly different at P < 0.05 by Duncan test.
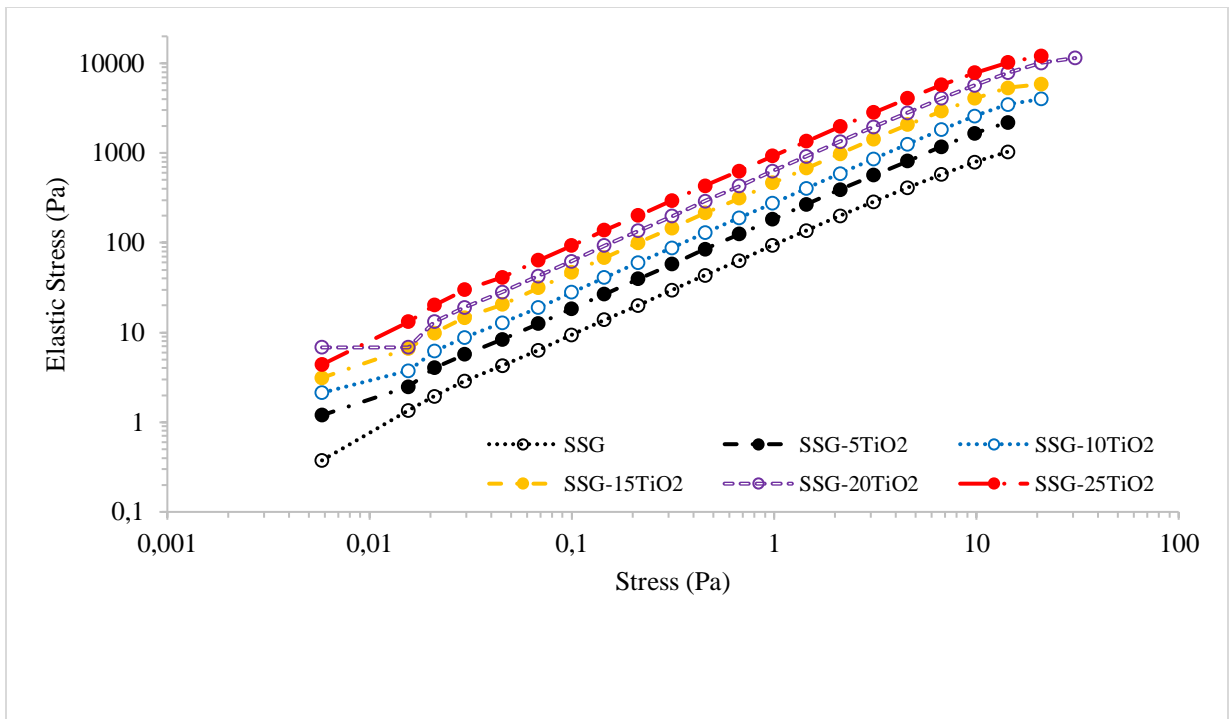
Table 5. Instrumental texture profile analysis (TPA) for 1% dispersion of sage seed gum (SSG) and SSG-TiO$_2$ nanocomposite hydrogels at 25 ℃.

Parameters/Samples	SSG	SSG-5TiO$_2$	SSG-10TiO$_2$	SSG-15TiO$_2$	SSG-20TiO$_2$	SSG-25TiO$_2$
Hardness (g)	255.1±3.2[b]	267.0±2.6[c]	320.4 ±5.7[d]	325.6±6.1[d]	307.2±3.8[c]	246.1±5.4[a]
Cohesiveness (-)	0.68±0.01[c]	0.63±0.01[b]	0.62±0.02[b]	0.56±0.01[a]	0.60±0.02[b]	0.62±0.03[b]
Adhesiveness (mJ)	12.5±0.5[c]	11.2±0.3[b]	13.2±0.1[d]	13.8±0.2[e]	12.3±0.4[c]	10.3±0.3[a]
Springiness (cm)	0.93±0.03[a]	1.12±0.01[d]	1.13±0.03[d]	1.03±0.03[c]	0.97±0.01[b]	0.92±0.01[a]
Gumminess (g)	173.1±4.0[b]	169.2±3.1[b]	199.2±2.8[d]	183.6±2.0[c]	185.7±2.2[c]	152.5±3.6[a]
Apparent elastic modulus (g/s)	106.4±2.4[b]	123.9±3.3[c]	136.0±4.2[d]	177.6±3.9[f]	142.5±2.0[e]	103.9±2.7[a]

Means followed by the different letters in the same rows are significantly different at P < 0.05 by Duncan test.
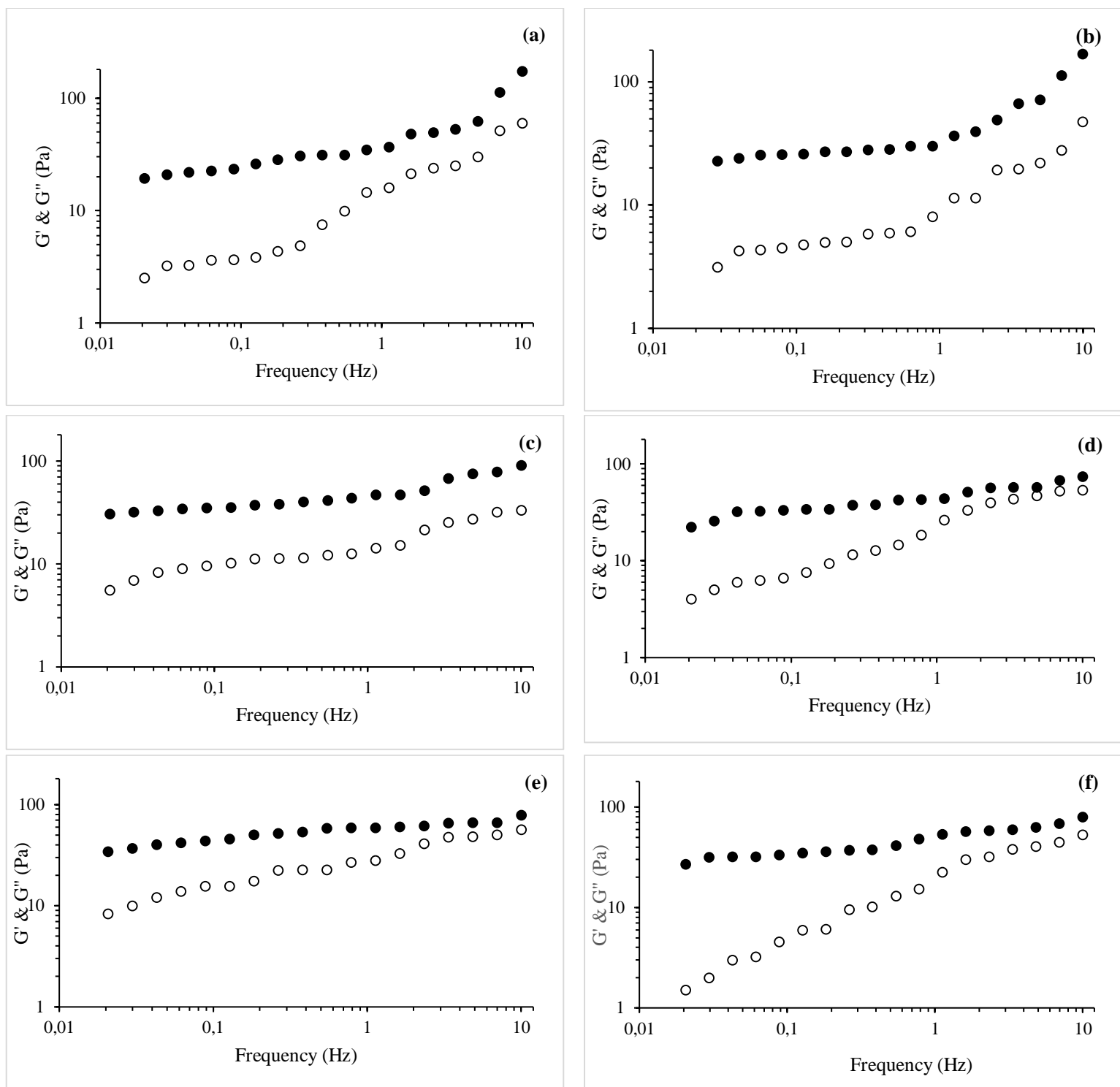
Fig. 1. Changes of G' (filled symbols) and G" (open symbols) in stress sweep of SSG (a), SSG-5TiO$_2$ (b),

SSG-10TiO$_2$ (c), SSG-15TiO$_2$ (d), SSG-20TiO$_2$ (e) and SSG-25TiO$_2$ (f) nanohybrid hydrogels (f = 1 Hz
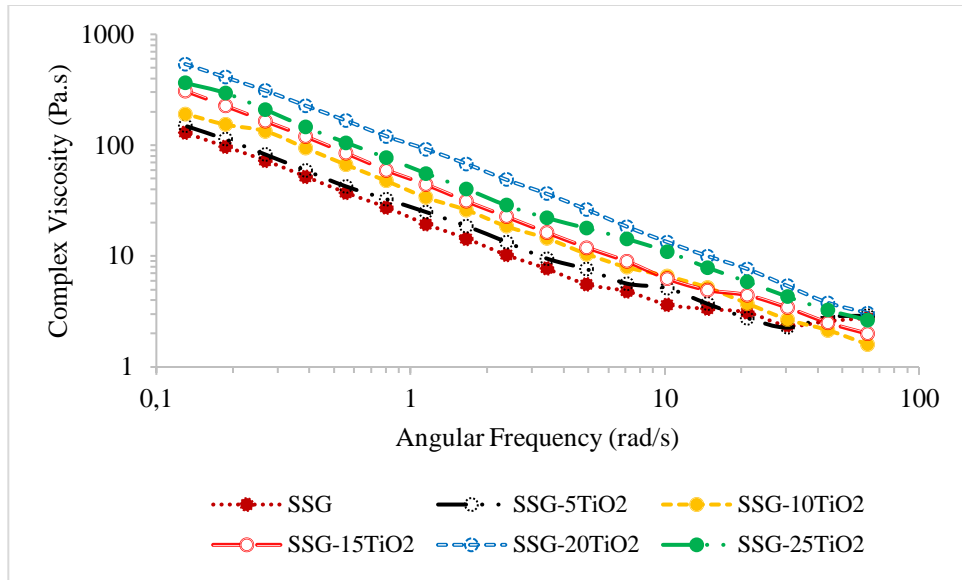
and T= 20℃).

Fig. 2. The Effect of increasing stress amplitude on elastic stress (G'.γ) of pure SSG and

TiO$_2$ reinforced SSG-based nanohybrid hydrogels.

Fig. 3. Frequency sweeps of G' (filled symbols) and G" (open symbols) for SSG (a), SSG-5TiO$_2$ (b), SSG-10TiO$_2$ (c), SSG-15TiO$_2$ (d), SSG-20TiO$_2$ (e) and SSG-25TiO$_2$ (f) nanohybrid hydrogels at LVE region (τ = 0.1 Pa) and T = 20 ℃.

Fig. 4. The effect of frequency on complex viscosity (η^*) of pure SSG and TiO_2 reinforced SSG-based

nanohybrid hydrogels at $\tau = 0.1$ Pa and T = 20 ℃.